Diagn Interv Radiol 2014; 20:316-322
© Turkish Society of Radiology 2014

INTERVENTIONAL RADIOLOGY
ORIGINAL ARTICLE

CT-guided percutaneous cryoablation of central lung tumors

Errol Colak, Servet Tatlı, Paul B. Shyn, Kemal Tuncalı, Stuart G. Silverman

PURPOSE
Cryoablation has been successfully used to treat lung tumors. However, the safety and effectiveness of treating tumors adjacent to critical structures has not been fully established. We describe our experience with computed tomography (CT)-guided percutaneous cryoablation of central lung tumors and the role of ice ball monitoring.

MATERIALS AND METHODS
Eight patients with 11 malignant central lung tumors (nine metastatic, two primary; mean, 2.6 cm; range, 1.0–4.5 cm) located adjacent to mediastinal or hilar structures were treated using CT-guided cryoablation in 10 procedures. Technical success and effectiveness rates were calculated, complications were tabulated and intraprocedural imaging features of ice balls were described.

RESULTS
All procedures were technically successful; imaging after 24 hours demonstrated no residual tumor. Five tumors recurred, three of which were re-ablated successfully. A hypodense ice ball with well-defined margin was visible during the first (n=6, 55%) or second (n=11, 100%) freeze, encompassing the entire tumor in all patients, and abutting (n=7) or minimally involving (n=4) adjacent mediastinal and hilar structures. Pneumothorax developed following six procedures (60%); percutaneous treatment was applied in three of them. All patients developed pleural effusions, with one patient requiring percutaneous drainage. Transient hemoptysis occurred after six procedures (60%), but all cases improved within a week. No injury occurred to mediastinal or hilar structures.

CONCLUSION
CT-guided percutaneous cryoablation can be used to treat central lung tumors successfully. Although complications were common, they were self-limited, treatable, and not related to tumor location. Ice ball monitoring helped maximize the amount of tumor treated, while avoiding critical mediastinal and hilar structures.

Department of Radiology (S.T. ✉ *statli@partners.org*), Brigham and Women's Hospital, Harvard Medical School, Boston, Massachusetts, USA.

Received 26 October 2013; revision requested 25 November 2013; revision received 3 December 2013; accepted 9 December 2013.

Published online 30 April 2014.
DOI 10.5152/dir.2014.13440

Malignant lung tumors represent a major cause of morbidity and mortality in developed nations (1). While surgical resection remains the treatment of choice for the local control of both non-small cell lung cancer and metastases to the lung, percutaneous image-guided ablative therapies, particularly heat-based ablation techniques such as radiofrequency (RF) ablation, have emerged as safe and effective alternatives in patients who are not surgical candidates (2–7). However, treatment of lung tumors using RF ablation presents technical challenges, including high electrical resistance of alveolar air, poor thermal conductivity of aerated lung, and the heat-sink effect of blood and air flow in well-perfused and aerated lung tissue (8, 9). In addition, RF ablation has a limited role in the treatment of tumors that are close to mediastinal and hilar structures (2–9). Since intraprocedural visualization of ablation zone margins is not possible during heat-based ablation procedures, treatment of central tumors could harm mediastinal and hilar structures, including the tracheobronchial tree. As a result, tumors close to central structures are generally not amenable to treatment using percutaneous heat-based ablation techniques (2–10). Also, RF ablation may interfere with conduction system of the heart and function of the pacemakers (11).

A growing body of literature describes the successful use of cryoablation in the treatment of malignancies in the liver, kidneys, and soft tissues (12–14). The ability to deploy multiple, individually-controlled cryoablation applicators facilitates the creation of ablation zones of desired shapes and sizes that can be tailored to the morphology of the tumor being ablated (15, 16). Cryoablation is also monitorable; ice balls can be visualized by computed tomography (CT) as a distinct ovoid area of low attenuation during the procedure. As a result, the treatment can be optimized while minimizing the risk of harming nearby critical structures (12–16). Also, cryoablation may be less painful than RF ablation (17). Finally, it has been suggested that cryoablation may be better suited for the treatment of thoracic tumors adjacent to the mediastinum because it spares the architecture of collagen-containing structures relative to RF ablation and enables preservation of the integrity of the tracheobroncheal tree (18). Heat-based ablation methods may not be safe in the treatment of central lung tumors because of a possibility of bronchial disruption or perforation, which may result in bronchopleural fistula formation (19). Although cryoablation has been used to treat lung malignancies (19–31), there are limited data on the safety and effectiveness of percutaneous cryoablation of central lung tumors. In this study, we describe our experience with CT-guided percutaneous cryoablation of central lung tumors and the role of ice ball monitoring.

Table 1. CT-guided percutaneous cryoablation of 11 central lung tumors adjacent to mediastinum and hilum

Age/ gender	Tumor type	Tumor size (cm)	Tumor location	AS	No. of applicators/ ice ball size (cm)	Tumor-AS distance	Ice ball-AS relation	Technical success	Recurrence	Complete ablation
60/F	Met (ACC)	3.1	LLL	LV	4/4.7	<1 cm	Abuts	+	No	Yes
60/F	Met (ACC)	2.0	LLL	Aorta	2/3.1	<1 cm	Abuts	+	No	Yes
60/F	Met (ACC)	2.1	RLL	RLL BVS	2/3.2	Abuts	Involves	+	Yes	Yes
58/F	Met (ACC)	2.8	LUL	LUL BVS	3/4.0	<1 cm	Involves	+	No	Yes
28/F	Met (ACC)	1.8	RML	RA	2/2.6	Abuts	Involves	+	No	Yes
46/M	Met (ACC)	2.4	LLL	LV	3/4.1	<1 cm	Abuts	+	Yes	Yes
46/M	Met (ACC)	1.0	Lingula	L BVS	1/2.0	<1 cm	Abuts	+	No	Yes
77/F	NSCLC	2.9	RUL	BCV & SVC	3/4.2	Abuts	Abuts	+	No	Yes
70/F	NSCLC	4.5	RUL	RV BVS	4/5.7	Abuts	Involves	+	Yes	No
47/M	Met (colon)	3.1	RUL	SVC & RUL BVS	3/4.3	Abuts	Abuts	+	Yes	No
56/F	Met (vagina)	4.2	LLL	LLL BVS	4/5.5	<1 cm	Abuts	+	Yes	Yes

AS, adjacent structure; Met, metastases; ACC, adenoid cystic carcinoma; LLL, left lower lobe; LV, left ventricle; RLL, right lower lobe; BVS, bronchovascular structures; LUL, left upper lobe; RML, right middle lobe; RA, right atrium; NSCLC, non-small cell lung carcinoma; RUL, right upper lobe; BCV, brachiocephalic vein; SVC, superior vena cava; RV, right ventricle.

Materials and methods

Patients

This study was conducted in compliance with the Health Insurance Portability and Accountability Act and was approved by our Institutional Review Board. Informed consent requirements to review images and medical records were waived. Between May 2006 and January 2009, 21 malignant lung tumors were treated using CT-guided percutaneous cryoablation. Of these, 11 tumors were located centrally, adjacent to the mediastinum (defined as being within 1 cm of the heart, hilum or other mediastinal bronchovascular structures) in eight patients (six females, two males; age range, 28.4–76.5 years; median age, 58.7 years). A total of 10 procedures were performed to treat these 11 tumors (Table 1). One patient had three metastatic tumors (two in one lung); each lung was treated in separate procedures. In another patient, two tumors located in the same lung (but different lobes) were treated in two separate procedures. Six patients had metastatic tumors (n=9) from adenoid cystic carcinoma of the salivary gland (n=7 tumors), squamous cell carcinoma of the vagina (n=1), and adenocarcinoma of the colon (n=1); while, two patients had primary non-small cell lung tumors. Patients were considered nonsurgical candidates due to the presence of multiple lung tumors (n=4), unresectability (n=2), poor pulmonary reserve (n=1), or synchronous hepatic metastases (n=1). The latter patient's liver metastasis was also cryoablated during the same procedure. None of the other patients had evidence of extrapulmonary metastases. A histopathological diagnosis was achieved in all patients either via surgery prior to the ablation (n=7) or biopsy during the ablation (n=1).

Tumor location

The tumors (mean, 2.6 cm; range, 1.0–4.5 cm) were located in the left lower lobe (n=4), right upper lobe (n=3), right lower lobe (n=1), right middle lobe (n=1), left upper lobe (n=1), or lingula (n=1). All 11 tumors either abutted (n=5) or were within 1 cm (n=6) of central structures, which included the hilum (n=5), left ventricle (n=2), right atrium (n=1), aorta (n=1), superior vena cava and right brachiocephalic vein (n=1), and both superior vena cava and hilar bronchovascular structures (n=1).

Cryoablation procedure

All patients fasted at least six hours prior to the procedure and underwent laboratory testing for complete blood count and coagulation factors. Percutaneous cryoablation procedures (n=10) were performed under general anesthesia, using an argon gas-based system (Cryohit; Galil Medical, Yokneam, Israel) and guided by a CT scanner equipped with fluoroscopy (Somatom Sensation Open, Siemens Medical Solutions, Forchheim, Germany). Infection prophylaxis was achieved by the intravenous administration of 1 g cefazolin sodium (Ancef, SmithKline Beecham Pharmaceuticals, Philadelphia, Pennsylvania, USA) at the beginning of the procedure and every eight hours for a total of 24 hours after the procedure. A warming system (Bair Hugger, Augustine Medical, Eden Prairie, Minnesota, USA) was used to maintain body temperature between 35°C and 37°C.

Following local anesthesia with 2% lidocaine and placement of a 22-gauge reference needle, one to four 17-gauge cryoablation applicators (mean, 2.8) were placed using tandem trocar technique. For the tumor with a diameter of 1 cm, one cryoablation applicator was placed centrally within the tumor; for all other tumors, applicators were placed approximately one centimeter from the tumor margin with tips positioned no more than 1.5 cm apart in the shape of a triangle or a diamond, depending on the size of the tumor and the number of the applicators used. Cryoablation was performed with two, 15–20-minute freezes separated by a 10-minute passive thaw. Intermittent, short, ice ball monitoring CT scans (120 kV, 120 mAs, and 5 mm slice thickness) were obtained every 3–5 minutes during freezing and following the passive thaw. Axial, coronal, and sagittal images were reformatted intermittently to further evaluate

whether the tumor was fully encompassed by the ice ball and whether the ice ball involved adjacent anatomic structures. During the treatment of three tumors, cryoablation applicators were repositioned to freeze more of the tumor (n=2) or avoid freezing critical structures (n=1). In three tumors freezing was reduced to as little as 20% of maximum capacity in the cryoablation applicators that were close to critical structures, to avoid their further involvement. In one tumor, freezing time was extended (n=1) so that the ice ball could encompass the entire tumor. Warm saline soaks were applied to the skin at the cryoablation applicator entry site to prevent skin injury. An unenhanced CT scan of the entire chest was performed following cryoablation applicator removal, to screen for complications.

Postprocedural care

All patients were admitted for overnight observation. Length of hospital stay ranged from one to four days (mean, 1.9 days). Complete blood count, serum creatinine, and serum myoglobin levels were evaluated at two and 24 hours following the procedure.

Thoracic magnetic resonance imaging (MRI) (n=9) (Signa Excite; GE Healthcare, Milwaukee, Wisconsin, USA) was obtained 24 hours after the procedure and repeated every three months during the follow-up (mean, 31.5 months; range, 3–62 months). MRI protocol included: transverse T2-weighted images with fast spin-echo (FSE) (TR/TE, 2400/90 ms), breath-hold fast-recovery FSE (1200–2996/91–94), and single-shot FSE (17240–53380/184–190); transverse T1-weighted images with a spin-echo sequence (500–800/14) or spoiled gradient-recalled echo (GRE) T1-weighted sequence (300–400/2.2–4.7); and transverse fat-suppressed T1-weighted dynamic images with a spoiled GRE sequence (260–435/4.2) or a fat suppressed three-dimensional fast-acquisition multiple-excitation spoiled GRE sequence (5.2–7.3/1.5–2.2), before and after the intravenous injection of 0.1 mmol/kg gadopentetate dimeglumine (Magnevist; Berlex Laboratories, Wayne, New Jersey, USA). MRI was contraindicated in one patient, who was followed using whole-body positron emission tomography (PET)-CT (Discovery ST, GE Healthcare) following intravenous injection of approximately 20 mCi ^{18}F-Fluoro-deoxy-glucose (FDG).

Image analysis

Two radiologists (14 and five years of experience) reviewed intraprocedural CT scans in consensus. Tabulated imaging features included the proximity of each ice ball to critical mediastinal and hilar structures, size and conspicuity of ice balls, and involvement of critical structures by ice balls. Both long and short dimensions of the ice balls were measured on axial images at the end of the second freeze and compared to tumor dimensions. The extent of peritumoral lung opacification (air-space consolidation in the lung parenchyma around the tumor) observed at each phase of the cryoablation procedure (applicator placement, first freeze, passive thaw, second freeze, active thaw) and on MRI or PET-CT 24 hours after the procedure, was categorized as minimal, segmental, multi-segmental, lobar, or involving all or most of a lung.

A treated tumor that showed no enhancement on MRI or no activity on PET-CT was considered completely ablated. New, remaining, or enlarging areas of focal enhancement or FDG-activity within or along the periphery of the ablation zone were considered evidence of local residual or recurrent tumor (32). A thin rim of enhancement or FDG-activity surrounding the ablation zone, commonly seen following ablation, was not considered evidence of residual or recurrent tumor (32). Ablation was considered technically successful if there was no sign of tumor on imaging performed 24 hours after the procedure. Primary effectiveness rate was defined as the percentage of tumors completely ablated after one procedure, with no sign of recurrence during the follow-up. Secondary effectiveness was defined as the percentage of tumors successfully ablated after one or two procedures (recurrent tumors that were ablated in a second procedure were included in the percentage).

Assessment of complications

Complications were recorded on a per-procedure basis and classified in accordance with the Common Terminology Criteria for Adverse Effects (CTCAE) of the National Cancer Institute (33). The presence, timing, severity, and treatment of pneumothoraces and pleural effusions that developed during the procedure were documented. Postprocedural laboratory changes including complete blood count, serum myoglobin, and creatinine levels were reviewed and any changes from the baseline were recorded.

Results

Technical success

All cryoablation procedures were technically successful. A hypodense ice ball with well-defined margins encompassed the entire tumor in all cases, and was visualized during the first freeze of six tumors (55%) and during the second freeze of all 11 tumors. Axial dimensions of the ice ball (mean, 3.9 cm; range, 2.0–5.7 cm) were larger (mean difference, 1.3 cm; range, 1.0–1.8 cm) than the corresponding dimensions of the tumors (mean, 2.6 cm; range, 1.0–4.5 cm). Ice balls increased progressively in size from first freeze to second freeze and either abutted (n=7) or minimally involved (n=4) adjacent mediastinal and hilar structures (Figs. 1, 2).

Peritumoral opacification was minimal following biopsy and cryoablation placement, but increased progressively during the freeze-thaw-freeze cycle and involved more than one segment in all procedures. The most marked change in peritumoral opacification occurred following the second freeze (Figs. 1, 2). Peritumoral opacification improved in all procedures after 24 hours, but remained multisegmental in four procedures.

Treatment effectiveness

Primary effectiveness rate was 55% (6/11) (mean follow-up, 31.5 months; range, 3–62 months). Five tumors adjacent to the hilar bronchovascular structures (n=4) or the heart (n=1) recurred in five patients, after a mean duration of 4.2 months (range, 3–7 months) following the cryoablation procedure (Table 1). Of these, three were re-ablated successfully (mean follow-up after the re-ablation procedure, 19 months; range, 6–36 months); thus, secondary effectiveness rate was determined as 82% (9/11). One patient declined additional treatment; another patient was not treated because of disease progression at other sites.

Complications

Pneumothorax developed in six procedures (60%) (Table 2). Four pnemothoraces developed during the procedures: two cases were minimal and were successfully managed by observation alone; one case was relieved by needle aspiration, and the other

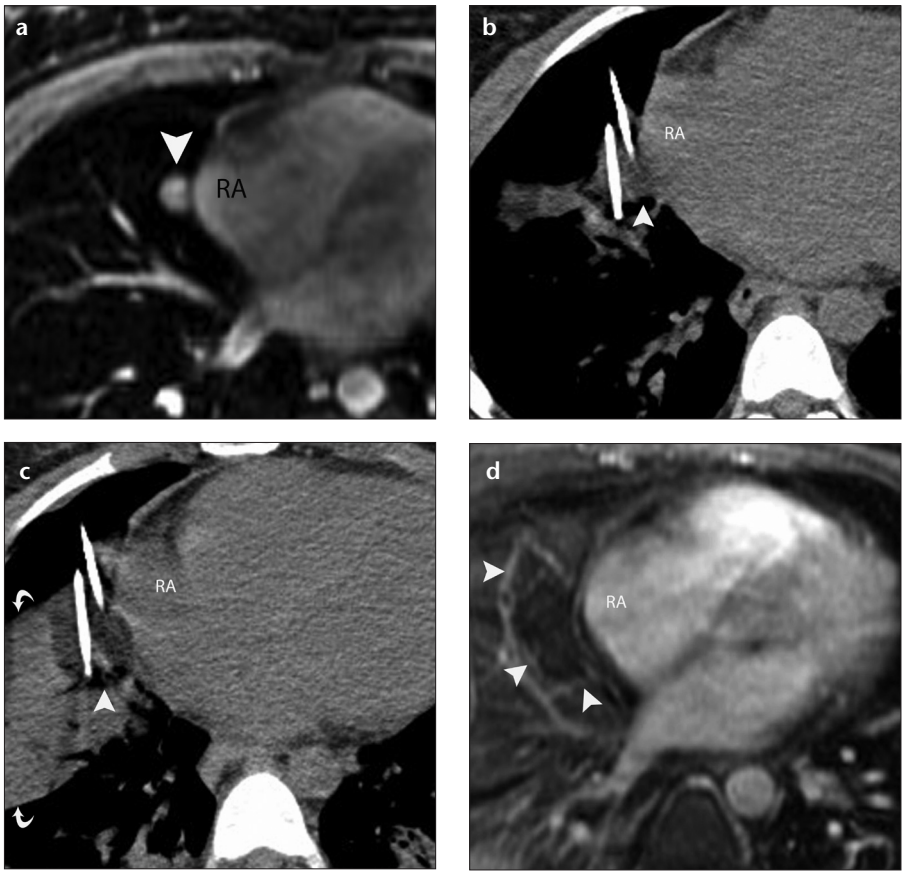

Figure 1. a–d. A 28-year-old woman with metastatic adenoid cystic neoplasm of the parotid gland to the lung treated using CT-guided percutaneous cryoablation. Axial fat-suppressed contrast-enhanced T1-weighted GRE MR image **(a)** demonstrates a 1.8 cm enhancing tumor *(arrowhead)* in the right middle lobe abutting the right atrium (RA). Axial CT scan **(b)** obtained during the first freeze shows that the ice ball *(arrowhead)* encompassed the right middle lobe tumor and abutted the wall of the RA. Eight minutes into the first freeze, the freezing capacity of the cryoablation applicator closest to the RA was reduced to 20% of the maximum capacity. Axial CT scan **(c)** obtained during the second freeze shows that the ice ball *(arrowhead)* encompassed the tumor completely and minimally involved the RA. Note extensive parenchymal opacification *(curved arrows)* that facilitates visualization of the ice ball. Subtracted fat-suppressed contrast-enhanced T1-weighted MR image **(d)** shows unenhanced cryoablation zones *(arrowheads)* and unaffected RA.

Table 2. Frequency and grade of complications following 10 CT-guided percutaneous cryoablation procedures in eight patients with 11 central lung tumors

Complications	No. of procedures	CTCAE grade	Comments
Pneumothorax (total)	6	-	-
Pneumothorax (asymptomatic)	2	1	No treatment
Pneumothorax (asymptomatic)	1	2	Manual aspiration
Pneumothorax (requiring catheter treatment)	3	2	Two delayed pneumothoraces in one patient
Respiratory distress (symptomatic)	1	4	Required reintubation
Pleural effusion (asymptomatic)	9	1	No treatment
Pleural effusion (symptomatic)	1	3	400 cc hemorrhagic fluid drainage
Hemoptysis	6	1	Self-limited, no treatment
Pain	3	1	Analgesic treatment
Pulmonary emboli	1	3	Anticoagulant treatment

CTCAE, Common Terminology Criteria for Adverse Effects.

case was managed by an 8 F loop catheter (Flexima, Boston Scientific, Natick, Massachusetts, USA) that was placed under CT-guidance and removed the next day. One patient required hospital readmission for delayed-onset pneumothorax that developed following discharge after two separate ablation procedures (recognized at six and seven days, respectively, following the ablations). Both pnemothoraces were successfully drained under CT-guidance.

In one patient, postprocedural hemoptysis and respiratory distress required reintubation. Bronchoscopy showed minimal bleeding at the carina. The patient was observed in the intensive care unit, improved with mechanical ventilation, and was discharged at day 4. Asymptomatic, segmental right lower lobe pulmonary emboli were identified on the 24-hour postablation follow-up MRI of a patient with a right upper lobe tumor. The emboli resolved after three months of anticoagulation. An ipsilateral, pleural effusion developed at 24 hours after all procedures; patients were asymptomatic and required no intervention except for one, whose baseline shortness of breath progressed and required CT-guided catheter drainage of 400 cc of hemorrhagic fluid. Transient hemoptysis occurred after six procedures (60%), but all cases resolved within a week without intervention (five, in three days; one, in six days). No cutaneous thermal injuries occurred at the puncture sites.

Postprocedural platelet and serum creatinine values were normal and unchanged compared to preprocedural levels, in all patients. White blood cell count slightly increased (mean increase, 3.7 K/μL; range, 0.5–11.2 K/μL) at two hours following all procedures, but exceeded normal levels following only four of the procedures. All white blood cell values returned to normal 24 hours later, except for a patient who had a large tumor (4.5 cm) ablated. This patient's mild leukocytosis (11–12 K/μL) was not accompanied by fever or other signs of infection and resolved within two days. Serum hematocrit levels decreased at two hours following all procedures (mean decrease, 3.6%; range, 1%–5%) and further decreased at 24 hours (mean decrease, 5.6%; range, 2%–7%). Serum myoglobin levels (mean, 443 μg/L; range, 104–803 μg/L) increased above normal (100 μg/L) after all procedures, except one;

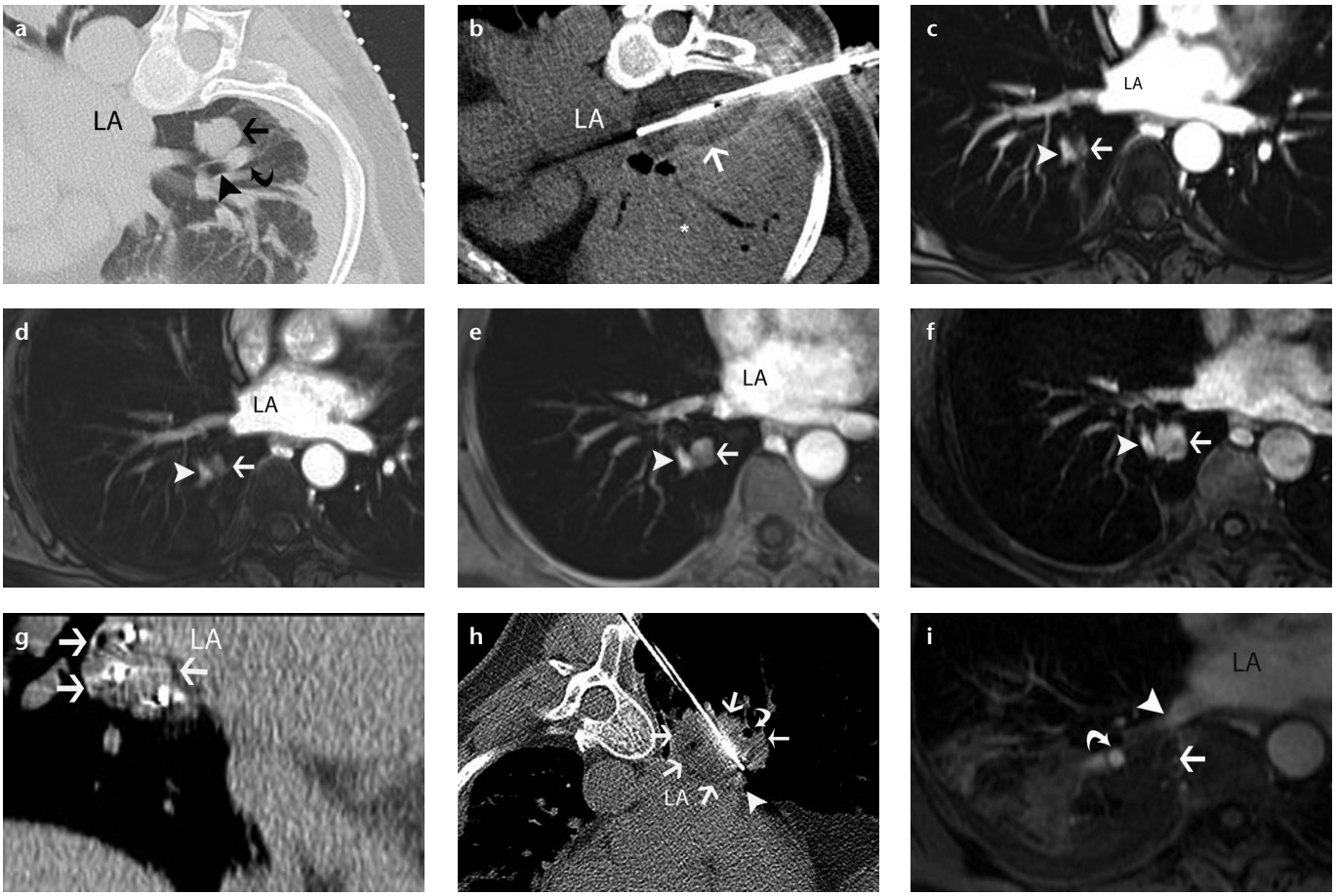

Figure 2. a–i. A 60-year-old woman with metastatic salivary gland adenoid cystic carcinoma to the lung treated by CT-guided percutaneous cryoablation. Axial CT scan **(a)** obtained during cryoablation of the right lower lobe pulmonary metastatic nodule *(arrow)*. Note the adjacent lower lobe bronchus *(arrowhead)* and pulmonary artery *(curved arrow)*. Axial CT scan **(b)** obtained during second freeze shows that the ice ball encompasses the nodule, involves the adjacent bronchus and pulmonary artery, and abuts the vertebra and the left atrium (LA). Note extensive peritumoral lung opacification *(asterisk)*. Axial fat-suppressed contrast-enhanced T1-weighted GRE MR images of the chest obtained at three **(c)**, six **(d)**, 12 **(e)**, and 18 months **(f)** show gradual growth of an enhancing soft tissue nodule *(arrow)* at the ablation site adjacent to the lower lobe pulmonary artery *(arrowhead)* consistent with a recurrence, which was treated percutaneously with another session of CT-guided cryoablation. Coronal reformation of CT scan **(g)** obtained following cryoablation applicator placement show peripheral location of three applicators within the tumor *(arrows)* in the shape of a triangle. Axial CT scan **(h)** obtained during freezing shows a low-attenuation ice ball *(arrows)* which covers the tumor and abuts the LA, pulmonary vein *(arrowhead)* and pulmonary artery *(thin arrow)* but involves the adjacent lower lobe bronchus *(curved arrow)*. Axial fat-suppressed contrast-enhanced T1-weighted GRE MR image **(i)** of the chest obtained 24 hours after the cryoablation demonstrates unenhanced ablation zone *(arrow)* and a patent pulmonary artery *(curved arrow)* and vein *(arrowhead)*.

abnormal levels returned to normal (n=3) or near normal (n=6).

Discussion

Our experience demonstrates that central tumors adjacent to critical structures such as the mediastinum, bronchial tree, heart, and great vessels can be treated successfully using CT-guided percutaneous cryoablation. Complications were common, but unrelated to the central location of the tumors and manageable. CT monitoring of the ice ball allowed us to maximize the chance of treating a tumor completely and avoid damaging adjacent critical structures. Intraprocedural ice ball monitoring enabled repositioning the applicators, prompted placement of additional ones, and allowed adjustment of freezing duration.

Prior reports have focused on the feasibility, safety, and local control rate of CT-guided cryoablation of lung tumors in general; however, these reports provided no detailed information regarding tumor location and did not discuss the issues relevant to the treatment of central tumors (19–31). Wang et al. (19) placed straight cryoablation applicators into tumors tandem to a guidance needle outside the CT gantry, as their CT gantry could not accommodate the entire length of straight cryoablation applicators. Freezing was initiated without scanning to confirm cryoablation applicator position and without CT monitoring of the ice ball. CT scans were obtained only after the cryoablation applicators were removed and the size of the ice balls was compared to that of the tumors. Central tumors were included; they were large (mean diameter, 6.4 cm) and treated only for local tumor control and palliation. As a result, tumors were only partially frozen. Despite the limited approach, brachial and recurrent laryngeal nerve damage developed in two patients. Our right-angle cryoablation applicators allowed CT scanning to occur with the applicators *in situ* so that the ice balls could be monitored. This allowed us to treat most tumors fully, without damage to central structures.

Our overall complication rate following lung tumor cryoablation was high, but comparable to others (21–23). Our

pneumothorax rate of 60% was similar to what has been reported following both cryoablation (range, 12%–61.7%) and RF ablation (range, 4.5%–61.1%) (19–21, 23, 34–36), and was likely related to the size and number of the applicators. However, the rate at which patients required catheter placement was slightly higher in our series (33%) relative to others (12%–18%) (19, 21, 23). Others have typically treated small pneumothoraces with needle aspiration rather than catheter insertion; this approach could have been used in our patients as well. The cause of delayed pneumothoraces following two separate procedures in one patient is unknown, but it was probably related to the patient rather than the procedure. Similar to other series (70%, 70.5%) (21, 23), pleural effusions were common but inconsequential, unless pulmonary function was already compromised. Hemoptysis was also common but transient. Length of hospital stay in our series (mean, 1.9 days) was similar to that seen after RF ablation of lung tumors (mean, 1.3 days; range, 1–6 days) (4, 37) and after lung cryoablations reported by others (mean, 2.6 days, range, 2–9 days) (8, 20).

We did not encounter bronchial injury despite involvement of bronchi in the ablation zone in six tumors. It has been proposed that the collagenous architecture of the tracheobronchial tree and hilar vasculatures are relatively resistant to the effects of cryoablation (38). Indeed, an endoluminal approach to the cryoablation of tracheobronchial malignancy has been shown to be safe (38–43). In a recent study, Zhikai et al. (44) described their findings regarding the treatment of unresectable central lung tumors with combined endobronchial and percutaneous cryoablation and airway stenting.

The "heat sink" effect of warm circulating blood undoubtedly helps protect the large central vascular structures during cryoablation (4). However, we believe that CT monitoring of the ice ball was also important in preventing vascular injury, as well as injury to other structures. For example, disruption of the tracheobronchial tree with fistula formation (10) and injury of the diaphragm (2) have been described following CT-guided percutaneous RF ablation, but they were not encountered in our series.

Biochemical and hematologic changes following cryoablation of lung tumors have not been described. Decreases in hematocrit level are expected and are likely due to combination of intraprocedural blood loss and hemodilution from administered fluids. Mild leukocystosis has been described following cryoablation of other sites such as the liver, likely reflecting a general inflammatory response to tissue necrosis rather than infection (45). We did not encounter thrombocytopenia, which is usually seen following liver cryoablation (45). Serum myoglobin levels increased after most procedures, however, not enough to prompt alkalinization of the urine (12–14). Cryoablation of muscles of the central airway or chest wall could have contributed to myoglobinemia.

Ice ball visibility was dependent on peritumoral lung parenchymal opacification. Although the underlying cause of peritumoral lung opacification is uncertain, animal studies have suggested that cryoablation results in capillary rupture and hemorrhage into alveolar spaces (46). Other investigators have suggested that hemorrhagic pulmonary edema occurs secondary to endothelial death (20). The marked and rapid improvement seen on MRI and CT after 24 hours suggests that the peritumoral lung opacification is predominantly due to hemorrhagic edema. In addition to allowing visualization of the ice ball, peritumoral lung opacification also increases thermal conductivity of lung tissue and allows for more rapid freezing and possibly larger ablation zones (28). Based on these observations, some authors have suggested an initial short freeze to create peritumoral opacification followed by two additional freezes to treat the tumor (20, 21, 23). One study showed that double- and triple-freeze protocols provided comparable ablation zones in a porcine model but the triple-freeze protocol resulted in earlier visualization of the ice ball. Therefore, a triple-freeze protocol may allow more effective intraprocedural ice ball monitoring in the future (28).

Peritumoral lung opacification during cryoablation is also important from a technical standpoint. When ablating multiple ipsilateral tumors during the same procedure (as in two of our procedures), cryoablation applicators should be placed in all tumors prior to freezing. If each tumor was cryoablated separately and sequentially, the peritumoral parenchymal opacification that develops around the first tumor might obscure other tumors and render placement of subsequent cryoablation applicators difficult.

We experienced five (45%) local recurrences. Four of these tumors were adjacent to the hilar bronchovascular structures and recurrence was likely due to the heat-sink effect (29). Placing more applicators close to the vessel causing the heat-sink effect and/or adding a third freezing cycle might have prevented this recurrence (20). We were able to successfully re-ablate three of five recurrences, yielding a secondary effectiveness rate of 82%, which is comparable to that of others (20, 29). Kawamura et al. (20) reported local recurrences in seven of 20 tumors (20%) in seven patients (35%) at 9–28 months (median, 21 months) follow-up. In a more recent series of 210 tumors, local tumor progression occurred in 50 patients (23.8%), with 1-, 2-, and 3-year technical effectiveness rates of 91.4%, 83%, and 83%, respectively (29). The authors demonstrated that larger tumor diameter (>2 cm) and presence of a ≥3 mm vessel within 3 mm of the tumor were significant risk factors for local recurrence (29).

We have used MRI in the surveillance of our patients following cryoablation of their lung tumors. Although MRI is frequently used to follow up patients undergoing cryoablation of kidney and liver tumors, it has not found widespread use in the follow-up of ablated lung tumors. We use MRI routinely in this clinical indication because of its superior soft tissue resolution, multiplanar capability, and lack of radiation. In addition to enhanced images, signal characteristics of tumors on traditional T1- and T2-weighted images provide better definition of ablation effect compared to other cross- sectional imaging modalities. Although, MRI is not an ideal tool to evaluate aerated lung parenchyma, its inherent superior soft tissue resolution allows excellent evaluation of ablated tumor, postablation residual changes, and recurrence.

The limitations of our study include its retrospective design, small sample size, and relatively short follow-up period for some patients. Other studies assessing RF ablation and cryoablation of lung tumors were also affected by the same limitations (3–8, 19, 20).

Although our sample size was small, our study was purposefully limited to patients with central tumors to determine the safety and effectiveness of cryoablation in this subset. However, our results are preliminary and further studies in larger groups of patients are necessary to warrant treatment safety and effectiveness.

In conclusion, our study results indicate that CT-guided percutaneous cryoablation of lung tumors adjacent to critical structures in the mediastinum and hilum can be successful. Although complications were common, they were self-limited, treatable, and unrelated to tumor location. Visualizing the ice ball helped treat the entire tumor and avoided damaging nearby critical structures.

Conflict of interest disclosure

The authors declared no conflicts of interest.

References

1. American Lung Association. American Lung Association Lung Disease Data 2008: 2008; 86.
2. VanSonnenberg E, Shankar S, Morrison PR, et al. Radiofrequency ablation of thoracic lesions: part 2, initial clinical experience--technical and multidisciplinary considerations in 30 patients. AJR Am J Roentgenol 2005; 184:381–390.
3. Belfiore G, Moggio G, Tedeschi E, et al. CT-guided radiofrequency ablation: a potential complementary therapy for patients with unresectable primary lung cancer--a preliminary report of 33 patients. AJR Am J Roentgenol 2004; 183:1003–1011.
4. Lee JM, Jin GY, Goldberg SN, et al. Percutaneous radiofrequency ablation for inoperable non-small cell lung cancer and metastases: preliminary report. Radiology 2004; 230:125–134.
5. Schaefer O, Lohrmann C, Langer M. CT-guided radiofrequency ablation of a bronchogenic carcinoma. Br J Radiol 2003; 76:268–270.
6. Ambrogi MC, Lucchi M, Dini P, et al. Percutaneous radiofrequency ablation of lung tumours: results in the mid-term. Eur J Cardiothorac Surg 2006; 30:177–183.
7. Simon CJ, Dupuy DE , Dipetrillo TA , et al. Pulmonary radiofrequency ablation: long-term safety and efficacy in 153 patients. Radiology 2007; 243:268–275.
8. Ahrar K, Littrup PJ. Is cryotherapy the optimal technology for ablation of lung tumors? J Vasc Interv Radiol 2012; 23:303–305.
9. Dupuy DE. Image-guided thermal ablation of lung malignancies. Radiology 2011; 260:633–655.
10. Yoon DH, Shim JH, Lee WJ, Kim PN, Shin JH, Kim KM. Percutaneous management of a bronchobiliary fistula after radiofrequency ablation in a patient with hepatocellular carcinoma. Korean J Radiol 2009; 10:411–415.
11. Rose SC, Thistlethwaite PA, Sewell PE, Vance RB. Lung cancer and radiofrequency ablation. J Vasc Interv Radiol 2006; 17:927–951.
12. Silverman SG, Tuncali K, Adams DF, et al. MR imaging-guided percutaneous cryotherapy of liver tumors: initial experience. Radiology 2000; 217:657–664.
13. Tuncali K, Morrison PR, Winalski CS, et al. MRI-guided percutaneous cryotherapy for soft-tissue and bone metastases: initial experience. AJR Am J Roentgenol 2007; 189:232–239.
14. Silverman SG, Tuncali K, vanSonnenberg E, et al. Renal tumors: MR imaging-guided percutaneous cryotherapy--initial experience in 23 patients. Radiology 2005; 236:716–724.
15. Tatli S, Acar M, Tuncali K, Morrison PR, Silverman S. Percutaneous cryoablation techniques and clinical applications. Diagn Interv Radiol 2010; 16:90–95.
16. Gangi A. How cool is percutaneous cryoablation? J Vasc Interv Radiol 2013; 24:821–822.
17. Allaf ME, Varkarakis IM, Bhayani SB, Inagaki T, Kavoussi LR, Solomon SB. Pain control requirements for percutaneous ablation of renal tumors: cryoablation versus radiofrequency ablation--initial observations. Radiology 2005; 237:366–370.
18. Ahmed A, Littrup P. Percutaneous cryotherapy of the thorax: safety considerations for complex cases. AJR Am J Roentgenol 2006; 186:1703–1706.
19. Wang H, Littrup PJ, Duan Y, Zhang Y, Feng H, Nie Z. Thoracic masses treated with percutaneous cryotherapy: initial experience with more than 200 procedures. Radiology 2005; 235:289–298.
20. Kawamura M, Izumi Y, Tsukada N, et al. Percutaneous cryoablation of small pulmonary malignant tumors under computed tomographic guidance with local anesthesia for nonsurgical candidates. J Thorac Cardiovasc Surg 2006; 131:1007–1013.
21. Inoue M, Nakatsuka S, Yashiro H, et al. Percutaneous cryoablation of lung tumors: feasibility and safety. J Vasc Interv Radiol 2012; 23:295–302.
22. Bang HJ, Littrup PJ, Currier BP, et al. Percutaneous cryoablation of metastatic lesions from non-small-cell lung carcinoma: initial survival, local control, and cost observations. J Vasc Interv Radiol 2012; 23:761–769.
23. Yamauchi Y, Izumi Y, Kawamura M, et al. Percutaneous cryoablation of pulmonary metastases from colorectal cancer. PLoS One 2011; 6:e27086.
24. Zhang X, Tian J, Zhao L, et al. CT-guided conformal cryoablation for peripheral NSCLC: initial experience. Eur J Radiol 2012; 81:3354–3362.
25. Yamauchi Y, Izumi Y, Hashimoto K, et al. Percutaneous cryoablation for the treatment of medically inoperable stage I non-small cell lung cancer. PLoS One 2012; 7:e33223.
26. Yamauchi Y, Izumi Y, Yashiro H, et al. Percutaneous cryoablation for pulmonary nodules in the residual lung after pneumonectomy: report of two cases. Chest 2011; 140:1633–1637.
27. Ito N, Nakatsuka S, Inoue M, et al. Computed tomographic appearance of lung tumors treated with percutaneous cryoablation. J Vasc Interv Radiol 2012; 23:1043–1052.
28. Hinshaw JL, Littrup PJ, Durick N, et al. Optimizing the protocol for pulmonary cryoablation: a comparison of a dual- and triple-freeze protocol. Cardiovasc Intervent Radiol 2010; 33:1180–1185.
29. Yashiro H, Nakatsuka S, Inoue M, et al. Factors affecting local progression after percutaneous cryoablation of lung tumors. J Vasc Interv Radiol 2013; 24:813–821.
30. Goto T, Izumi Y, Nakatsuka S, Nomori H. Percutaneous cryoablation as a salvage therapy for local recurrence of lung cancer. Ann Thorac Surg 2012; 94:e31–33.
31. Pusceddu C, Sotgia B, Fele RM, Melis L. CT-guided thin needles percutaneous cryoablation (PCA) in patients with primary and secondary lung tumors: a preliminary experience. Eur J Radiol 2013; 82:e246–253.
32. Smith S, Gillams A. Imaging appearances following thermal ablation. Clin Radiol 2008; 63:1–11.
33. National Cancer Institute. Common Terminology Criteria for Adverse Events 2010; version 4.03, June 14. Available at: http://ctep.cancer.gov/protocolDevelopment/electronic_applications/ctc.htm. Accessed January 29, 2013.
34. Thanos L, Mylona S, Pomoni M, et al. Percutaneous radiofrequency thermal ablation of primary and metastatic lung tumors. Eur J Cardiothorac Surg 2006; 30:797–800.
35. Suh RD, Wallace AB, Sheehan RE, Heinze SB, Goldin JG. Unresectable pulmonary malignancies: CT-guided percutaneous radiofrequency ablation--preliminary results. Radiology 2003; 229:821–829.
36. Fernando HC, De Hoyos A, Landreneau RJ, et al. Radiofrequency ablation for the treatment of non-small cell lung cancer in marginal surgical candidates. J Thorac Cardiovasc Surg 2005; 29:639–644.
37. Gadaleta C, Mattioli V, Colucci G, et al. Radiofrequency ablation of 40 lung neoplasms: preliminary results. AJR Am J Roentgenol 2004; 183:361–368.
38. Sanderson DR, Neel HB, Fontana RS. Bronchoscopic cryotherapy. Ann Otol Rhinol Laryngol 1981; 90:354–358.
39. Mathur PN, Wolf KM, Busk MF, Briete M, Datzman M. Fiberoptic bronchoscopic cryotherapy in the management of tracheobronchial obstruction. Chest 1996; 110:718–723.
40. Moorjani N, Beeson JE, Evans JM, Maiwand MO. Cryosurgery for the treatment of benign tracheo-bronchial lesions. Interact Cardiovasc Thorac Surg 2004; 3:547–550.
41. Maiwand MO. The role of cryosurgery in palliation of tracheo-bronchial carcinoma. Eur J Cardiothorac Surg 1999; 15:764–768.
42. Asimakopoulos G, Beeson J, Evans J, Maiwand MO. Cryosurgery for malignant endobronchial tumors: analysis of outcome. Chest 2005; 127:2007–2014.
43. Gage AA, Baust J. Mechanisms of tissue injury in cryosurgery. Cryobiology 1998; 37:171–186.
44. Zhikai Z, Lizhi N, Liang Z, et al. Treatment of central type lung cancer by combined cryotherapy: Experiences of 47 patients. Cryobiology 2013; 67:225–229.
45. Nair RT, Silverman SG, Tuncali K, Obuchowski NA, vanSonnenberg E, Shankar S. Biochemical and hematologic alterations following percutaneous cryoablation of liver tumors: experience in 48 procedures. Radiology 2008; 248:303–311.
46. Izumi Y, Oyama T, Ikeda E, Kawamura M, Kobayashi K. The acute effects of transthoracic cryoablation on normal lung evaluated in a porcine model. Ann Thorac Surg 2005; 79:318–322.